J. Coat. Technol. Res., **21** (2) 481–492, 2024
https://doi.org/10.1007/s11998-023-00874-4

ORIGINAL RESEARCH

Numerical and experimental investigation on formation of the film for different die lip configurations in lithium-ion battery electrode slot-die coating

Xiaosong Gong, Jie Han, Fei Yan, Xiaozhong Du

Received: 6 April 2023 / Revised: 7 October 2023 / Accepted: 21 October 2023

Abstract The slot-die coating is the most commonly used manufacturing method for producing lithium-ion battery electrodes. However, how to achieve high surface consistency for electrodes still confronts one challenge. In this research, the slot coating processes with different die lip configurations were carefully investigated using numerical and experimental methods. The motion pattern, internal flow structure of the coating bead, and coating uniformity were explored during the coating process of lithium battery cathode slurry. The low-flow limit at different coating gaps was also determined by combining the viscous capillary model and numerical methods, which was in good agreement with experimental results. The results showed that a smaller coating gap controlling the upstream meniscus between the upstream die lip and slot exit was favorable to the coating uniformity. For the same thickness films, a larger coating gap was apt to increase formation of edge defects. However, the coating speed had little effect on the edge height. The evolution of flow structure for the coating bead (parabolic–sharp angle–diagonal) under different processes was investigated by tracking the particle trajectories during the coating process. It can provide theoretical guidance for the fabrication of high-quality electrodes.

X. Gong, J. Han, X. Du (✉)
School of Mechanical Engineering, Taiyuan University of Science and Technology, Taiyuan 030024, China
e-mail: xiaozhong_d@163.com

F. Yan
College of Automobile Engineering, Wuhan University of Technology, Wuhan 430070, China

X. Du
School of Energy and Materials Engineering, Taiyuan University of Science and Technology, Taiyuan 030024, China

Keywords Slot-die coating, Low-flow limit, Edge defect, Meniscus fluctuation, Particle distribution

Introduction

Slot-die coating is widely used for manufacturing lithium-ion battery electrodes due to its advantages such as pre-metered coating and high coating speed, making it a versatile and low-waste coating technology.[1] During the coating process, the liquid confined in the coating gap by the upstream and downstream menisci forms a coating bead, and the upstream meniscus of the coating bead displaces air in the dynamic contact line of mobile foils. The film is formed at the downstream meniscus. If the flow state of the coating bead is not stable, various defects will inevitably occur during the coating process, such as ribbing, dripping, rivulets, and air entrainment.[2] The presence of defects leads to a dramatic deterioration in the electrochemical performance of lithium-ion battery electrodes.[3] Since the lithium battery slurry is a particle suspension with high viscosity, the appropriate range of process parameters can only be determined through a large number of experiments, which will undoubtedly increase the production cost. The performance of the electrode depends on the uniformity of macroscopic surface and internal microstructure of the coating. The uniformity of the wet coating and its particle distribution will be affected by different flow structures. Therefore, it is important to study the flow law of the slurry during the coating process from different macroscopic and microscopic perspectives.

One of the main problems in the slot-die coating process is to determine the range of process parameters that stabilize the coating. Much research has been done theoretically. Ruschak[4] carried out a theoretical study based on the film coating theory of Landau and Levich[5] and proposed the first capillary model for

predicting the stability of the coating process. Higgins and Scriven[6] extended Ruschak's work by proposing a viscous capillary model that takes into account viscous effects and allows upstream meniscus movement, providing coating windows for various geometric and operating conditions (e.g., coating gap, coating speed, and flow rate). Since then, some models, such as Carreau-type fluids,[7] power-law fluids,[8,9] and inertial viscous capillary model,[10] were proposed by many scholars to adapt different fluid properties. Yoon et al.[11] developed a simplified viscous capillary model by omitting the downstream pressure step in the viscous capillary model. Carvalho and Kheshgi[12] proposed that the minimum film thickness was related to the critical capillary number. Chang et al.[13] used an experimental approach to discover three regions that affected the minimum film thickness as well as the dominant influencing factors in each region. The viscous capillary prediction model provides a basic theoretical prediction model for practical production, but it cannot visualize the real state of fluid motion.

With the development of computational fluid dynamics, two-dimensional (2-D) numerical models have been widely used to quickly predict the range of process parameters for defect-free and stable coating.[1,8,14–17] Tan et al.[18] analyzed the flow mechanism at the trailing edge of intermittent slot coating. Bhamidipati[19,20] investigated the flow behavior of shear-thinning fluids at different process parameters using 2-D numerical models. The different 2-D numerical models can provide solutions for optimizing the coating process, but they also have limitations. The kinetic analysis of the 2-D numerical model in the coating process is based on the assumption that the coating thickness is uniformly distributed along the transverse direction. However, depending on the geometry of the slot coating die and the coating conditions, the fluid velocity may be different along the transverse direction. The different flow characteristics lead to different defects and coating uniformity. Thus, a three-dimensional (3-D) computational fluid dynamics model needs to be further investigated on the flow pattern of the fluid during the coating process. Huang et al.[21] investigated the generation mechanisms of three different types of defects in the coating process through 3-D numerical simulations. Kim et al.[22] used a 3-D numerical model to optimize the stable coating conditions and the geometry of the slot coater. Jung and Nam[23] analyzed the effect of periodic inlet disturbances on the 3-D transient flow of the fluid inside the coating head chamber. Thus, the 3-D fluid dynamics model can provide a comprehensive demonstration of the fluid motion and thus provide a powerful tool to reveal the flow pattern of the slurry in different dimensions during the coating process.

The flow under the die lip is the sum of the flow driven by pressure (Poiseuille flow) and the shear-driven flow of the moving substrate (Couette flow). The balance between these two different flow structures ultimately determines the position of the upstream and downstream menisci. Furthermore, the combination of flow structures influences the quality of the coating as well as the distribution of the particles. Aggregation of large particles may block the coating gap with consequences for the stability of the coating process.[24] Moreover, the microstructure of electrode coating particles influences the final performance of the cell.[25] Pan et al.[26] proposed a particle coating window that provides a guiding scheme for the production of defect-free wet films with uniform thickness and particle dispersion. Carvalho's group[27–29] found that shear-driven migration dominates particle transportation in slot coating, which is the main reason for particle inhomogeneous distribution and agglomeration. Therefore, it is important to further understand the evolution of the internal flow structure for the coating bead as well as its influence on particle distribution.

In short, in the coating process, the flow mechanism of the coating bead has not been fully understood due to the complexity of the rheological properties and process parameters of lithium battery slurry. The stability of the downstream meniscus guarantees the consistency of the final film thickness, but the motion patterns of its surface and influencing factors have rarely been mentioned by scholars. Therefore, to solve the above issues, this study proposes to investigate the flow mechanism of the coating bead by numerical and experimental methods.

Numerical method

Governing equations

During the slot coating process, as shown in Fig. 1, the flow of the coating bead is a three-dimensional, transient, incompressible laminar gas–liquid two-phase flow. The interface between air and anode slurry is traced using the volume of fluid method (VOF).[30] The VOF model can describe two or more immiscible fluids by solving a set of momentum equations and tracking the volume fraction of each fluid over the entire region. A brief list of the control equations considered in the model is given below.

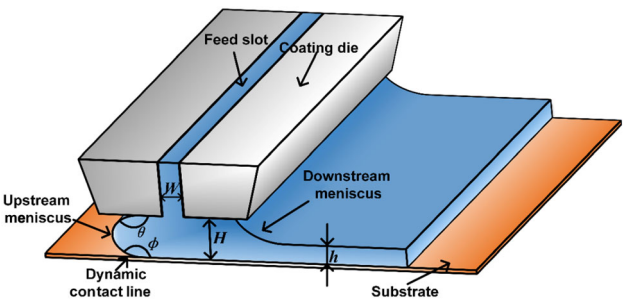

Fig. 1: Schematic diagram of slot-die coating principle

The incompressible two-phase flow is shown in the following equation:

$$\alpha_i + \alpha_a = 1 \tag{1}$$

where α_i and α_a represent the volume fraction of air and cathode slurry, respectively. When $\alpha_i = 1$ or 0, it means filled with anode slurry or air.

The volume fraction equations of liquid and vapor phases can be written as follows:

$$\frac{\partial a_i}{\partial t} + \nabla \cdot (\vec{v} a_i) = \frac{\dot{m}_i}{\rho_i} \tag{2a}$$

$$\frac{\partial a_a}{\partial t} + \nabla \cdot (\vec{v} a_a) = \frac{\dot{m}_a}{\rho_a} \tag{2b}$$

where $\dot{m}_i = -\dot{m}_a$. Momentum equations can be written as follows:

$$\frac{\partial}{\partial t}(\rho \vec{v}) + \nabla \cdot (\rho \vec{v} \vec{v}) = -\nabla p + \nabla \cdot \left[\mu\left(\nabla \vec{v} + \nabla \vec{v}^{\mathrm{T}}\right)\right] + \rho \vec{g} + \vec{F} \tag{3}$$

where $\vec{F}$ is the surface tension converted to volume force by the continuous surface force model.

$$\vec{F} = \sigma \frac{a_i \rho_i k_i \nabla a_i + a_a \rho_a k_a \nabla a_a}{0.5(\rho_i + \rho_a)} \tag{4}$$

where σ and k denote the surface tension coefficient and the interface curvature, respectively. The interface curvature k can be calculated from:

$$k = \nabla \cdot \hat{n} \tag{5}$$

$$\hat{n} = \hat{\boldsymbol{n}}_{\mathbf{w}} \cos\theta_w + \hat{\boldsymbol{t}}_{\mathbf{w}} \sin\theta_w \tag{6}$$

where $\hat{\boldsymbol{n}}_{\mathbf{w}}$ is the unit vector normal to the wall and $\hat{\boldsymbol{t}}_{\mathbf{w}}$ is the unit vector tangential to the wall. θ_w is the contact angle between the anode slurry and the wall.

The Fluent-DPM (discrete phase model) part allows the simulation of moving particles as moving mass points, where abstractions are used for the shape and volume of the particles. Based on Newton's second law, the ordinary differential equations that govern the particle motion are represented as follows:

$$m \frac{\mathrm{d}\vec{v}}{\mathrm{d}t} = \vec{F}_{\mathrm{drag}} + \vec{F}_{\mathrm{pressure}} + \vec{F}_{\mathrm{virtual\_mass}} + \vec{F}_{\mathrm{gravitation}} + \vec{F}_{\mathrm{other}} \tag{7a}$$

$$\frac{\mathrm{d}x}{\mathrm{d}t} = \vec{v} \tag{7b}$$

where $\vec{F}_{\mathrm{drag}}$ is the fluid traction, $\vec{F}_{\mathrm{pressure}}$ is the pressure on the particle, $\vec{F}_{\mathrm{virtual\_mass}}$ is the mass force, and $\vec{F}_{\mathrm{gravitation}}$ is the gravity of the particle.

Numerical model and boundary conditions

The computational domain and boundary conditions are shown in Fig. 2. H is the coating gap, and in this study, the coating gap H varies between 0.25 and 0.35 mm, and the die lip inclination angle β is 135°. Nonuniform cell distributions in the x–y plane are used to reduce the computation cost. More cells are generated in the coating gap, as shown in Fig. 3. Uniform cell distributions are used in the z-direction. The 3-D model is applied to do quantitative verification in the different flow states as well as study the transverse motion pattern of the wet film. The 2-D model with an arbitrary x–y cross section of the 3-D computational domain is used to predict the low-flow limit under different slot gaps. The 2-D model has no periodic boundary condition (BC5). Other boundary conditions are consistent with the three-dimensional model, and the mesh division is consistent with Fig. 3a.

Then, the flow structure of the coating bead was investigated by changing the die lip configuration of the two-dimensional model, as shown in Fig. 4, where overbite and underbite die configurations have the same minimum coating gap as the Normal die configuration.

BC1: Velocity inlet.

BC2: No-slip and penetration wall boundary conditions are specified. The contact angle between the slurry and the stationary wall surface is set to 50°.

BC3: Standard atmospheric pressure outlet.

BC4: A moving wall condition is imposed at this location. The contact angle between the anode slurry and the moving wall is set to 60°.

BC5: A periodic boundary condition is set at the side walls.

The capillary effect has little effect on the edge height of the wet film.[31] Therefore, we used the periodic boundary conditions to study the overall velocity distribution pattern of the downstream menis-

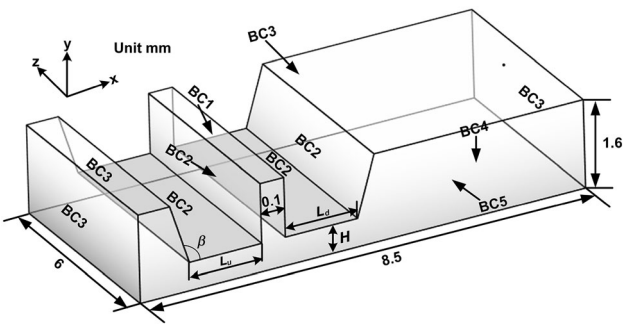

Fig. 2: 3-D slot coating computational domain boundary conditions and sizes

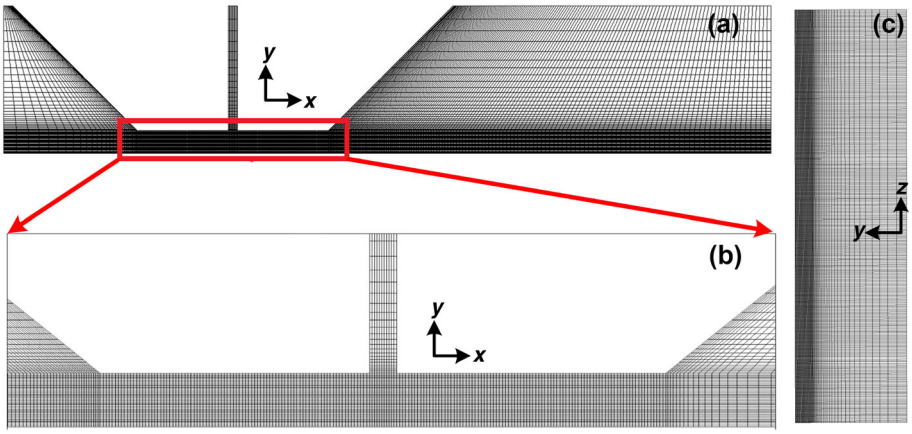

Fig. 3: Computational domain meshing method: (a) front view; (b) zoomed-in local view; and (c) left view

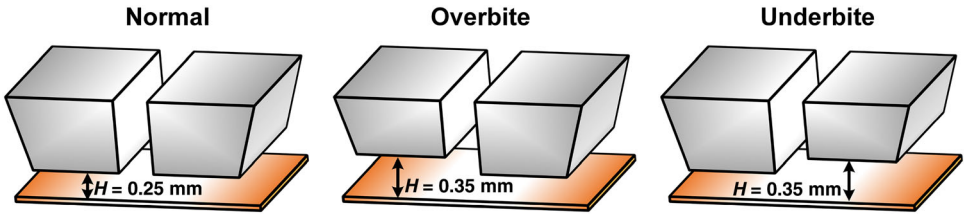

Fig. 4: Schematic diagram of three different slot-die configurations

cus. Considering the performance of shear thinning of lithium battery anode slurry, the power-law model ($\tau = K \cdot (\mathrm{d}u/\mathrm{d}y)^n$) is used as the principal model to describe the viscosity of the pseudoplastic fluid, where τ is the shear viscosity, K is the consistency coefficient, $\mathrm{d}u/\mathrm{d}y$ is the shear rate, and n is the fluidity coefficient. In this model, according to the experimental results, the value of n is 0.37 and the surface tension is 0.0417 N/m. In this study, the CICSAM method is used to construct the free interface, and the Couple method is used for solving the discrete pressure–velocity coupling equation with the time step set to 10^{-4}, where the continuity residuals are less than 10^{-3} to ensure the accuracy of the model. The Fluent discrete phase model (DPM) is used to track the particle trajectory. The model does not take into account the interaction between particles and the effect of particles on the flow field in the area of the coating bead. The performance of particles is set to inert particles. The DPM particle motion will not affect the flow field of the continuous phase around the DPM particles.

Viscous capillary model

The viscous capillary model can be used to predict the position of the upstream meniscus and the state of the coating bead. The basic mechanism defining the low-flow limit can be well described by the viscous capillary model, which is derived by Lee et al.[8] and is used in this paper as follows:

$$x_\mathrm{u} - x_\mathrm{f} = -\frac{1}{ka}\left(P_\mathrm{d} - P_\mathrm{v} - 1.34\mathrm{Ca}^{2/3}\frac{\sigma}{h_\infty} - (x_\mathrm{d} - x_\mathrm{f})kb - \frac{\sigma}{h_\mathrm{u}}(\cos\theta + \cos\phi)\right) \tag{8}$$

where

$$\mathrm{Ca} = \frac{k(U_\mathrm{web}/H)^{n-1}U_\mathrm{web}}{\sigma} \tag{9a}$$

$$a = \left[\frac{U_\mathrm{web}(n+1)(2n+1)}{n}\right]^n H^{-n-1} \tag{9b}$$

$$b = \left[\frac{U_\mathrm{web}(H-2h_\infty)(n+1)(2n+1)}{n}\right]^n H^{-(2n+1)} \quad \text{for } h_\infty < H/2 \tag{9c}$$

$$b = -\left[\frac{U_\mathrm{web}(2h_\infty - H)(n+1)(2n+1)}{n}\right]^n H^{-(2n+1)} \quad \text{for } h_\infty > H/2 \tag{9d}$$

Here, x_u denotes the upstream meniscus position, x_f is the slot exit position, H is the coating gaps, σ is the surface tension, U_web is the web speed, $P_\mathrm{d} - P_\mathrm{v}$ is the difference between ambient pressures downstream and upstream, called bead pressure ($P_\mathrm{d} - P_\mathrm{v} = 0$), and h_∞ is the wet thickness.

Results

Low-flow limits at different coating gaps

As shown in Fig. 5, the low-flow limits for lithium battery anode slurry are derived at different coating gaps using a 2-D numerical model and a viscous capillary model. The coating speed (U_{web}) at which bubbles occur in the wet film is the maximum coating speed (representing the low-flow limit). It can be seen that the viscous capillary model and the two-dimensional numerical model provide an appropriate prediction of the process parameter range. However, at high Ca numbers, the results of the viscous capillary model show some deviation. This is caused by the viscous capillary model neglecting the inertia effect.[10] In addition, three regions of minimum wet thickness of the wet film were found to exist. According to the research of Chang et al.,[13] in region I (Ca is approximately less than 1), h_{min} increases with an increase in Ca. At this time, surface tension is the main driving force. In region II (Ca is approximately 1-3.1 in this work), it is independent of Ca. With an increase in Ca, the effects of the capillary force decrease, and the inertial force induced by the slurry supply is relatively small. Therefore, the viscous force becomes the only dominant force driving the slurry flow. In region III (Ca greater than 3.1), the minimum wet thickness can be seen to decrease with the increase of Ca. At this time, the viscous and inertial forces are the dominant forces driving the slurry flow.

When the slot gap is less than or equal to twice the film thickness, from equation 9a, Ca increases with the increase of flow rate and coating speed, resulting in a more stable coating bead and delaying the generation of air entrainment defects.[10,21,32] Finally, a smaller h_{min} or a larger coating speed can be obtained; this is because the coating bead has sufficient pressure to sustain itself against the air entrainment at a high Ca. However, the extended coating window in the high-inertia/capillary region cannot be infinitely large. The coating speed above a critical value can result in dynamic wetting failure.[2]

A smaller coating gap allows for a greater range of stable coating process conditions. In addition, when the slurry flows in a smaller coating gap, it is easier to produce thinner coatings due to the behavior of the shear-thinning fluid.

Wet coating thickness profile and uniformity

As shown in Figs. 6 and 7, the results of the 3-D computational model well show the flow state of the wet coating under different operating conditions. As shown in Fig. 6a, when the upstream meniscus just reaches the edge of the upper die lip, the thickness is about 245 μm, which is considered as having reached the high-flow limit. For stable coating, as shown in Fig. 6b, the thickness is about 194 μm in this case. When air entrainment occurs, as shown in Fig. 6c, a large amount of air is involved in the film and the film's lateral thickness changes drastically. In addition, the minimum coating thickness seems to be no less than 125 μm. According to the study of the low-flow limit shown in Fig. 6c, when the capillary number is sufficiently high, the effect of viscous force will be much more significant than surface tension force. At this time, h_{min} depends only on the downstream coating gap and is independent of capillary number. Thus, the capillary effects have been ignored. By applying lubrication theory to the upstream and downstream channels, minimum wet thickness of the wet film without vacuum is about half of the coating gap.[6]

The transverse thickness distribution of the films under different slot gap conditions is shown in Fig. 7. When the coating gap is raised to 0.3 mm, the upstream meniscus is pulled near the exit of the slot, and the thickness of the film in the transverse direction slightly vibrates in this case, as shown in Fig. 7b. While it keeps going up 0.35 mm, as shown in Fig. 7c, the specified thickness could not be achieved. It also can be

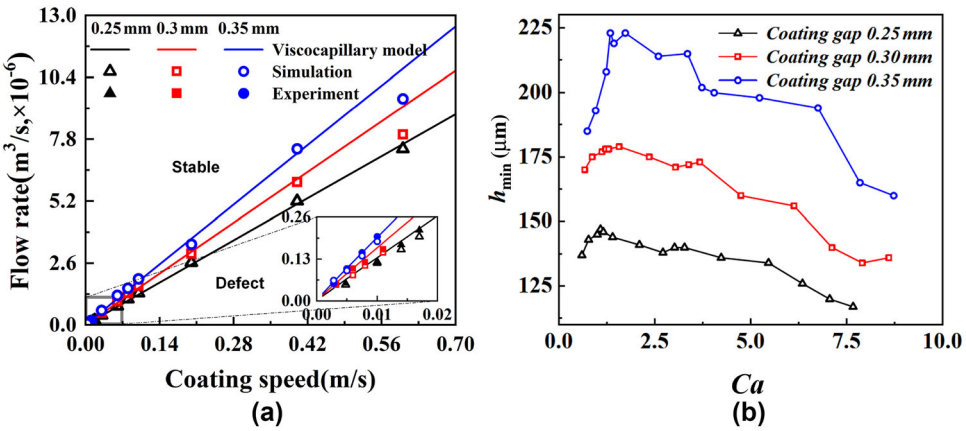

Fig. 5: Low-flow limits and h_{min} for different coating gaps: (a) low-flow limits and (b) h_{min}

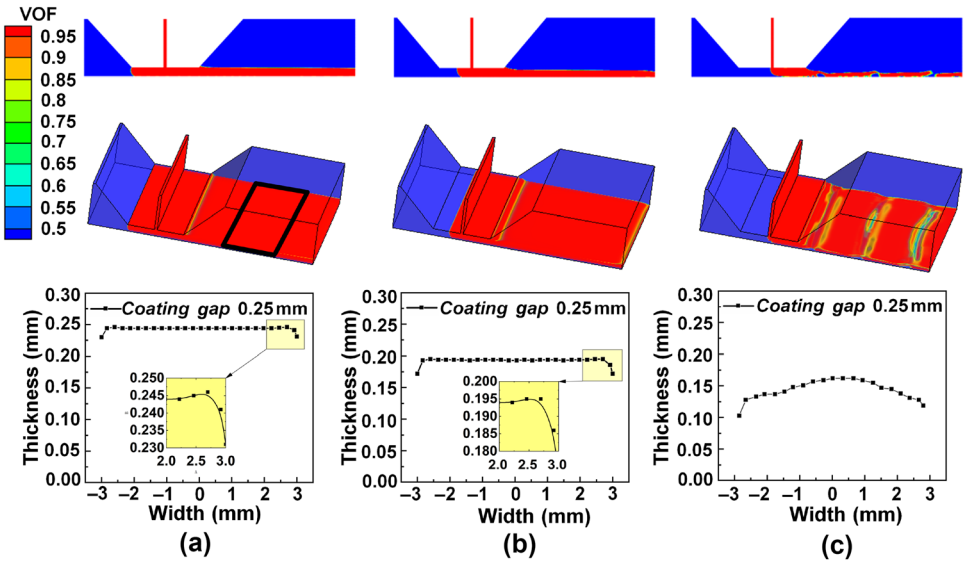

Fig. 6: 3-D simulation results under different operating conditions: (a) U_{ln} = 0.126 m/s, U_{web} = 0.05 m/s; (b) U_{ln} = 0.04 m/s, U_{web} = 0.02 m/s; and (c) U_{ln} = 0.02 m/s, U_{web} = 0.017 m/s

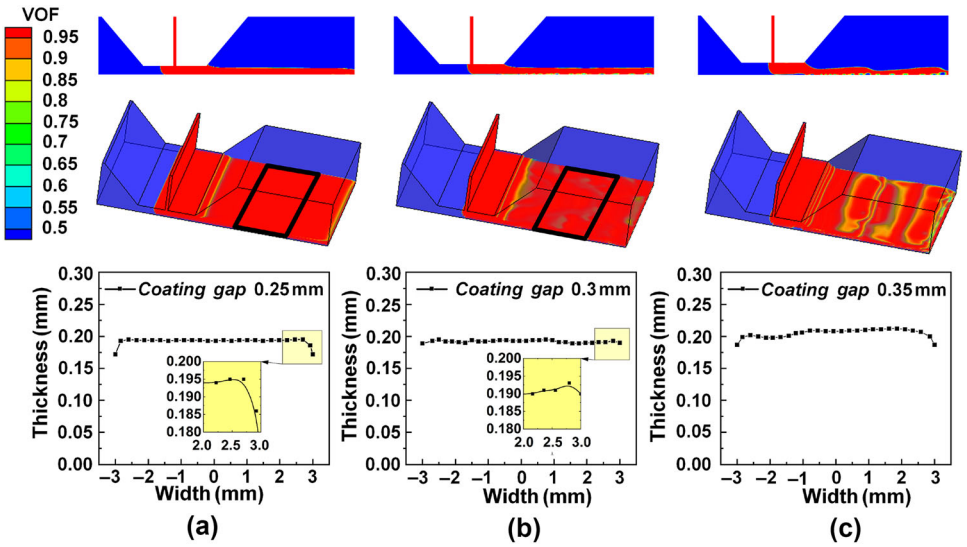

Fig. 7: 3-D simulation results under different coating gaps: (a) U_{ln} = 0.04 m/s, U_{web} = 0.02 m/s; (b) U_{ln} = 0.04 m/s, U_{web} = 0.0215 m/s; and (c) U_{ln} = 0.04 m/s, U_{web} = 0.017 m/s

observed that the edge height during stable coating is smaller than that during near-air case. That is, through an increased gap height at constant film heights, the neck-in in the upper film also increases. A larger gap ratio will result in a higher wet film edge height.[31,35] In contrast, a decreasing coating gap results in a decreasing draw ratio of coating speed and average flow velocity below the die lips. When the coating speed is too high and exceeds a certain critical stretch ratio, the film thickness shows a sinusoidal variation. The corresponding simulation is shown in Fig. 7c.

As shown in Fig. 8, in order to observe the distribution of wet film thickness along the coating direction as well as to avoid the chance of thickness distribution, we selected the wet film on the x–y plane at $Z = -2, -1, 0$, and 1 mm to observe the fluctuation in thickness. It can be seen that the best uniformity is observed when the coating gap is 0.25 mm for reaching the specified thickness of the film. When the slot gap was raised to 0.3 mm, the thickness at this time produced slight fluctuations along the coating direction. Continuing to raise the slot gap to 0.35 mm resulted in sharp fluctuations in thickness. Therefore, when the upstream meniscus reaches the exit of the die lip, the effect of instability in the coating bead region on the thickness fluctuation is global. The thickness in both length and width directions is adversely affected at this point.

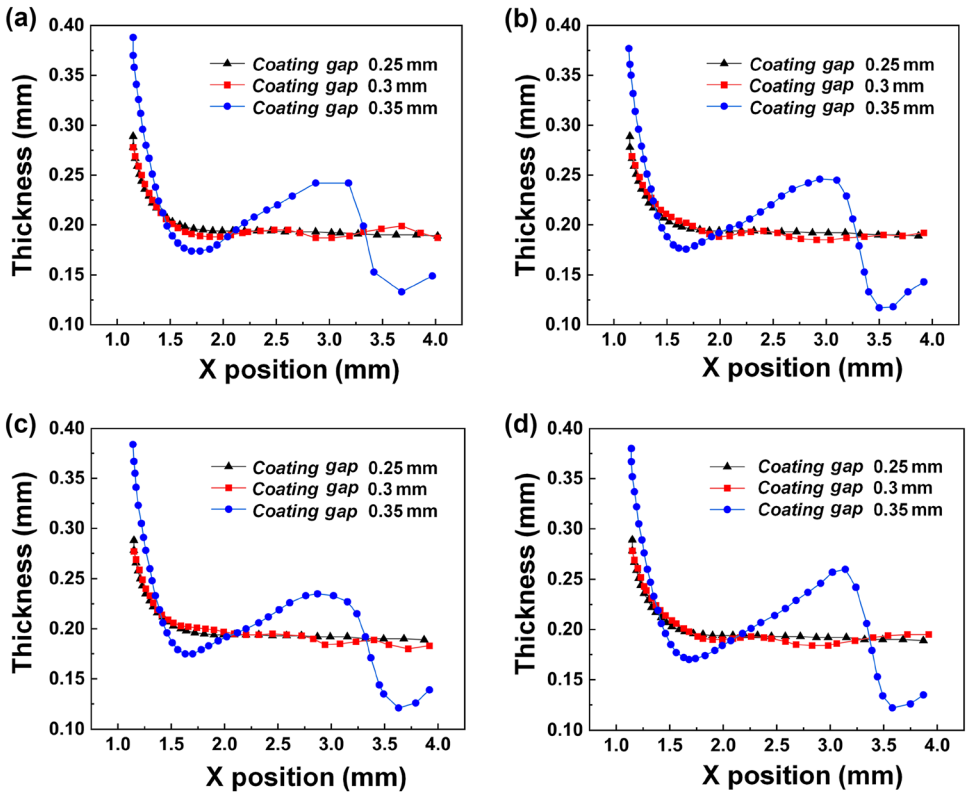

Fig. 8: Wet film thickness under different coating gaps (0.25, 0.3 and 0.35 mm) at the *x*–*y* planes: (a) *Z* = − 2 mm; (b) *Z* = − 1 mm; (c) *Z* = 0 mm; and (d) *Z* = 1 mm

The overall film uniformity is likewise one of the important results to be observed. The uniformity of a wet film is calculated by introducing a uniformity index. The uniformity index represents the variation of the specified variable on the surface, where the highest uniformity has a value of 1. The area-weighted uniformity of the specified field variable is calculated using the area-weighted formula, Index γ_a:

$$\gamma_a = 1 - \frac{\sum_{i=1}^{n}\left[\left(\left|\phi_i - \overline{\phi}_a\right|\right)A_i\right]}{2\left|\overline{\phi}_a\right|\sum_{i=1}^{n} A_i} \tag{10a}$$

$$\overline{\phi}_a = \frac{\sum_{i=1}^{n} \phi_i A_i}{\sum_{i=1}^{n} A_i} \tag{10b}$$

where i is the facet index of a surface with n facets, A_i is the mesh surface area, and $\overline{\phi}_a$ is the average value of the field variable over the surface.

The direction of substrate movement (coating direction) is X. The X position coordinate of the slot exit center is $X = 0$ mm. The length of the die lip is 1 mm, so the X coordinate of the right edge of the die lip is 1 mm. The black box region chosen for this study is the region of stable coating; specifically, the black boxed area between 2 and 4 mm along the coating direction (Figs. 6 and 7) was selected to calculate the area-weighted uniformity index of the film thickness. The film uniformity index is 0.993 when the upstream meniscus reaches the edge of the die lip (Fig. 6a), 0.995 between the die lips (Fig. 7a), and 0.989 near the slot exit (Fig. 7b). Thus, a smaller coating gap should be chosen and the upstream meniscus should be controlled between the upstream die lips when manufacturing films of the same thickness.

The experimental results obtained using the same process parameters of Fig. 7 are shown in Fig. 14. The thickness profile along the dashed line inside the red box of Fig. 14 was measured, and the dashed lines are the midline along the coating direction and the width direction, respectively. The wet film thickness is measured with a wet film wheel. The average wet thickness of the three measurements was 190 μm at a slot gap of 0.25 mm and 200 μm at 0.35 mm. The experimental results are about 4% different from the simulation results. From the dry film thickness profiles shown in Fig. 14, it can be seen that the thickness distribution of the coating surface fluctuates when the slot gap is raised to 0.3 mm. Through an increased gap height at constant film heights, the neck-in in the upper film also increases. Hence, the heavy edges should move toward the center of the film and increase in height and width. When the slot gap is raised to 0.35 mm, the specified thickness cannot be reached.

Velocity profiles

In order to investigate motion patterns of the downstream meniscus, three special flow states (near-leaking, stable and near-air) were selected to study the velocity profile at different locations of the downstream meniscus. From Fig. 9a and b, under the near-leaking condition, it can be seen that the velocity component at both edges is fairly fast along the outward direction. The stable state also has a similar but mild velocity component. However, the maximum velocity under both conditions was nearly the same. The velocity of the wet film edge was little affected by the coating speed, which is comparable to the results of Schmitt et al.[31] for ''thick edge'' defects. In the near-air case, as shown in Fig. 9c, the velocity component of the slurry produces sharp fluctuations in the transverse direction. For an increased coating gap, the region affected by the edge of the coating expands toward the center of the film, which may be caused by the drawing action.

As shown in Fig. 10a, in the near-leaking case, the transverse velocity at the position of the bottom of the downstream meniscus still fluctuates, but it is close to zero when stably coated (Fig. 10b). It can be observed that the edge velocity during stable coating is smaller than that during near-leaking. According to the conclusion by Schmitt et al.[31] and Spiegel et al.,[33] the coating speed does not have a significant effect on the formation of edge height. When the leaking condition is reached, the larger inlet flow rate results in a higher gap pressure. The higher pressure pushes the wet film to expand in the lateral direction, which in turn leads to a higher velocity in the edge region. As shown in Fig. 6, the edge height of the wet film when the leaking condition is reached is not the same as that of the wet film under the stable coating condition. Therefore, the formation mechanism of edge defects may be related to the pressure-driven lateral movement of the wet film surface, not only the gap ratio.

Figure 11 shows the transverse velocity distributions at 0.5 mm from the bottom of the downstream meniscus. As shown in Fig. 11a and b, the two edge velocity components are still present in the near-leaking case. The motion pattern of the downstream meniscus is highly correlated with the position of the upstream meniscus. Different positions of the upstream meniscus may lead to different velocity profiles of the downstream meniscus, which in turn may have an impact on the film uniformity.

Generally speaking, the formation of the edge height is related to the transverse velocity profile of the downstream meniscus. When the limiting operating conditions (near-leaking and near-air) are reached, it results in velocity fluctuations of the downstream meniscus. This results in a film that develops higher edge height and nonuniformity. Therefore, controlling the upstream meniscus between the die lips will be more beneficial to film uniformity.

Coating bead flow structure

The evolution of the flow structure for the coating bead under different processes was explored by tracking the particle trajectories during the coating process. The Fluent-DPM model has been used to track the particle trajectories

As shown in Fig. 12a, the evolution of the flow structure can be observed from the high-flow limit to the low-flow limit. The necessary condition for stable coating is that the Poiseuille flow exactly counteracts the Couette flow formed by the relative motion of the substrate and the die head. The sum or subtraction of the Poiseuille flow and the Couette flow results in a pure flow rate for the preset inlet flow.[34] In the near-leaking case, it is mainly a pressure-driven Poiseuille flow. The particle distribution is approximately parabolic. As a result, the substrate is moving at a relatively small speed, resulting in a large accumulation of particles under the upstream die lip. In the stable coating state, the parabolic particle distribution becomes sharp-angled due to the shearing effect of the Couette flow. In the case of air entrainment, the flow pattern changes to Couette flow dominant. The particle distribution becomes diagonal under the strong shearing effect of Couette flow, and at this time, the substrate moves at faster speed, leading to excessive dragging force. When the die lip is set to overbite, as shown in Fig. 12b, the upstream meniscus is shifted to

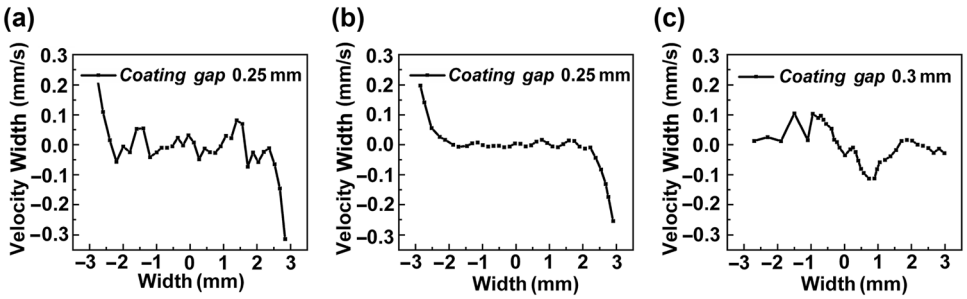

Fig. 9: Width–directional velocity profiles at the middle of downstream meniscus: (a) U_{In} = 0.126 m/s , U_{web} = 0.05 m/s; (b) U_{In} = 0.04 m/s, U_{web} = 0.02 m/s; and (c) U_{In} = 0.04 m/s, U_{web} = 0.0215 m/s

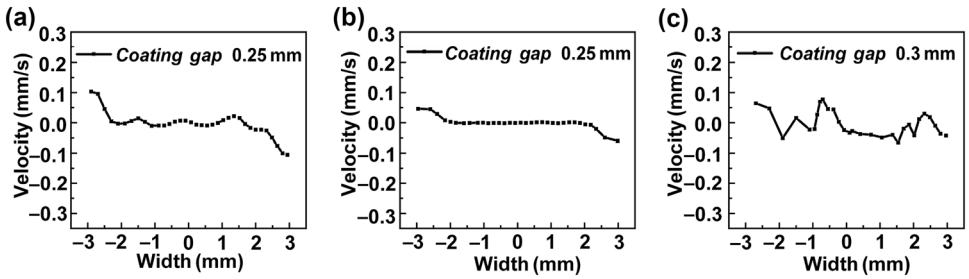

Fig. 10: Width–directional velocity profiles at the bottom of downstream meniscus: (a) U_{In} = 0.126 m/s, U_{web} = 0.05 m/s; (b) U_{In} = 0.04 m/s, U_{web} = 0.02 m/s; and (c) U_{In} = 0.04 m/s, U_{web} = 0.0215 m/s

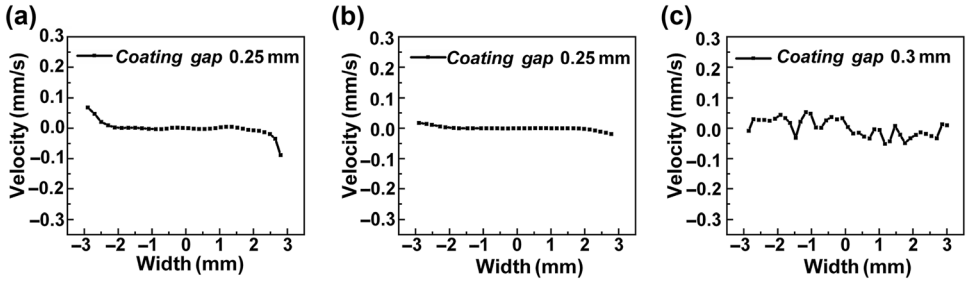

Fig. 11: Width–directional velocity profiles at 0.5 mm along the bottom of meniscus: (a) U_{In} = 0.126 m/s, U_{web} = 0.05 m/s; (b) U_{In} = 0.04 m/s, U_{web} = 0.02 m/s; and (c) U_{In} = 0.04 m/s, U_{web} = 0.0215 m/s

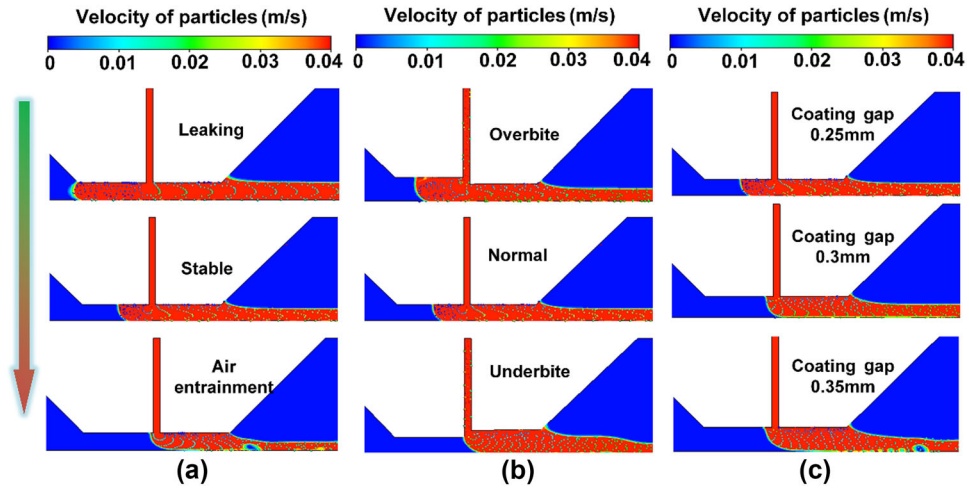

Fig. 12: Particle trajectory distributions under different operating conditions: (a) U_{In} = 0.126 m/s, U_{web} = 0.05 m/s; U_{In} = 0.04 m/s, U_{web} = 0.02 m/s; and U_{In} = 0.02 m/s, U_{web} = 0.017 m/s, (b) U_{In} = 0.04 m/s, U_{web} = 0.02 m/s, and (c) U_{In} = 0.04 m/s, U_{web} = 0.02 m/s; U_{In} = 0.04 m/s, U_{web} = 0.0215 m/s; and U_{In} = 0.04 m/s, U_{web} = 0.017 m/s

the left, allowing for greater coating speed of the moving substrate. An increase in the upstream coating gap could not change the downstream flow structure, but too much increase can create vortexes. The particles are trapped in the circulating vortex, which can lead to particle agglomeration and be unfavorable to particle uniform dispersion.[35] When the die lip is set to underbite, the upstream coating gap and pressure gradient are smaller, resulting in lower pressure in the coating bead. The flow structure shifts to Couette flow dominance. Figure 12c shows that an increase in the coating gap promotes the combination of Poiseuille flow and Couette flow to transform into Couette flow when the same thickness was reached at different slot gaps. It can be seen that the particles are more uniformly distributed by the shearing effect of the Couette flow, but too large a coating gap can entrap the film into the air.

In summary, during the process from the high-flow limit to the low-flow limit, the flow structures of the coating bead undergo a ''parabolic–sharp angle–diagonal'' transformation. The overbite die lip configura-

tion increases the maximum coating speed. An increase in the coating gap encourages the combination of Poiseuille flow and Couette flow to become Couette flow. For coating the same thickness of film with a coating gap less than or equal to twice the wet film thickness, the effect of the coating gap can be explained by the pressure gradient under the downstream die lip. The effect of the coating gap can be interpreted by the pressure gradient underneath the downstream die lip. The coating flow from the feeding slot gap to the coating gap could be regarded as the pipe flow with contraction or expansion geometry. With a larger coating gap, namely an expansion in the pipe, the kinetic energy would convert to the static pressure energy.[26] At this point, the pressure gradient is lower and the Couette flow pattern is more likely to dominate, which is more conducive to uniform particle dispersion.

Experimental settings

The slot coating experimental platform is shown in Fig. 13, which shows the slot coater. It is equipped with a high-precision syringe pump and motorized abutment. The table is equipped with a heating element capable of controlling the temperature from room temperature to 120 °C. Figure 13b shows a picture of the slot-die head with a maximum coating width of 50 mm. The anode slurry was dispersed in a planetary centrifugal mixer (Kejing, MSK-SFM-16) at 300 rpm. The mixing process lasted for 90 min. Then, a copper foil of mass M_1 is coated with a little wet paste. The sum mass of wet paste and copper foil is M_2. Finally, it is dried to a constant weight. The mass of copper foil and dry coating is M_3.

Then the solid content η of the anode slurry is expressed by the following equation:

$$\eta = (M_3 - M_1)/(M_2 - M_1) \times 100\% \quad (11)$$

The calculated η is equal to 48.5%. The lithium battery anode slurry is delivered to the slot-die head with a high-precision syringe pump. The coating gap is adjusted by two screw micrometers on the top of the head frame with a high-precision micrometer. The slot gap W of the die head is adjusted to 0.1 mm by a shim. During the coating experiments, when defects were observed to appear, the coating speed and inlet flow rate at that time were recorded. We then measured the thickness of the wet film using a wet film wheel. In order to verify the uniformity of the films, drying to constant weight after the coating operation was completed. We verified the surface uniformity by measuring the thickness profile of its surface with a digital multimeter and repeated each experiment five times. The corresponding experimental results are shown in Fig. 14.

Conclusions

In this research, slot coating with different die lip configurations was investigated by numerical and experimental methods. The motion pattern, internal flow structure of the coating bead, and coating uniformity were analyzed in the coating process. Three main conclusions were drawn as follows.

i. During the coating process, the viscous capillary model and the two-dimensional numerical model provided an appropriate prediction of the process parameter range. However, at high Ca numbers, the results of the viscous capillary model showed some deviation. This was caused by the viscous capillary model neglecting the inertia effect. In addition, three regions were observed Ca-h_{min}-based stable coating window. The dominant force driving the slurry in each region was associated with the relative magnitudes of the capillary, viscous, and inertial forces. The results revealed that a smaller minimum coating thickness could be obtained for a lower coating gap.

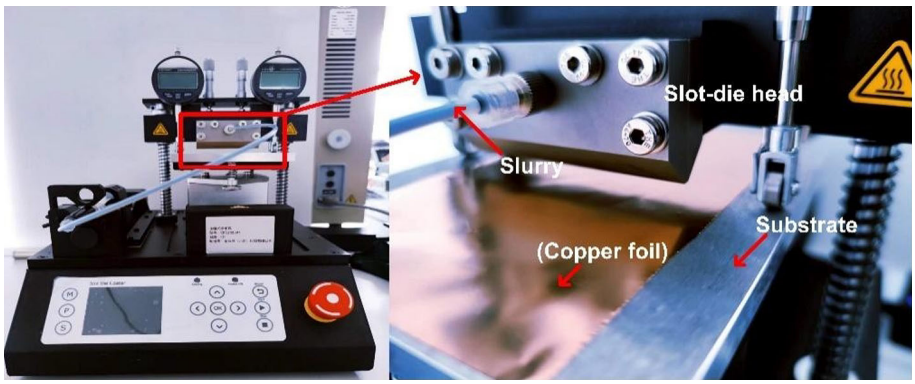

Fig. 13: Slot-coating experiment platform

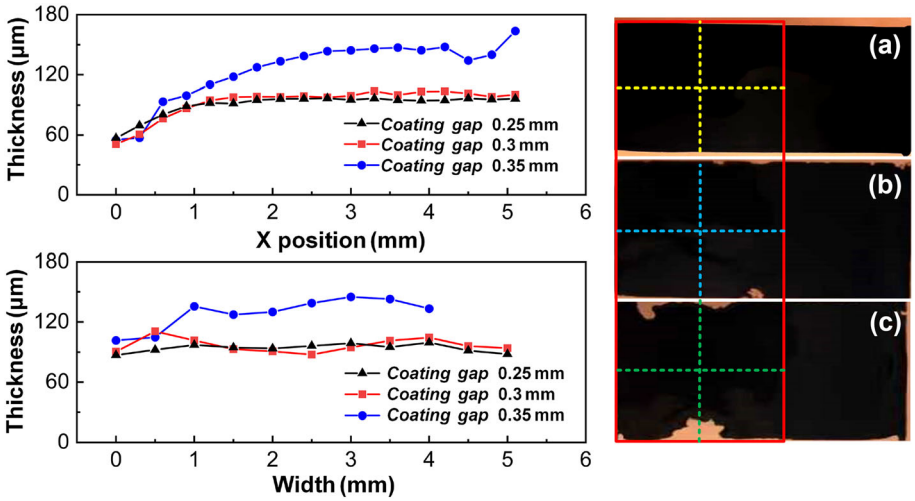

Fig. 14: Measured dry film thickness at different coating gaps: (a) coating gap = 0.25mm, U_{ln} = 0.04 m/s, U_{web} = 0.02 m/s; (b) coating gap = 0.30mm, U_{ln} = 0.04 m/s, U_{web} = 0.0215 m/s; and (c) coating gap = 0.35mm, U_{ln} = 0.04 m/s, U_{web} = 0.017 m/s

ii. The velocity profiles on the surface of the meniscus under different operating conditions were investigated using a 3-D computational fluid dynamics model. The results revealed that the stability of the downstream meniscus was affected when the near-leaking and near-air condition occurred. A smaller coating gap controlling the upstream meniscus between the upstream die lip and slot exit was more beneficial for film uniformity. In addition, this study provided a partial qualitative explanation for the generation of the thick edge defect by analyzing the transverse velocity profiles of the downstream meniscus. For films of the same thickness, a larger coating gap could intensify the formation of edge defects. The coating speed had little effect on the edge height. However, due to the simplification of the boundary conditions, there was still a discrepancy with the actual situation. In further research, a more accurate model will be developed to study the edge flow in the coating process.

iii. The evolution of flow structure for the coating bead under different processes was investigated by tracking the particle trajectories during the coating process. It was observed that the flow structure inside the coating bead changed from parabolic to sharp angle to diagonal during the process from high-flow limit to low-flow limit. An increase in the coating gap would also induce a change in the flow structure. Couette flow could be preferable for uniform particle dispersion. Overbite die lip configuration could obtain a large coating speed, but improper control could generate a vortex easily.

In future work, more experiments and numerical simulations will be performed to understand the edge defect formation mechanism in the slot coating process and the effect of particles on the actual coating process.

Acknowledgments The work was supported by grants from the Research Project Supported by Shanxi Scholarship Council of China (Grant No: 2021-137) and Fundamental Research Program of Shanxi Province (Grant No: 202103021224273).

Conflict of interest The authors have no competing interests to declare that are relevant to the content of this article.

References

1. Creel, EB, Tjiptowidjojo, K, Lee, JA, et al. "Slot-Die-Coating Operability Windows for Polymer Electrolyte Membrane Fuel Cell Cathode Catalyst Layers." *J. Colloid Interface Sci.*, **610** 474–485 (2022)
2. Ding, X, Liu, J, Harris, TAL, "A Review of the Operating Limits in Slot Die Coating Processes." *AICHE J.*, **62** (7) 2508–2524 (2016)
3. Mohanty, D, Hockaday, E, Li, J, et al. "Effect of Electrode Manufacturing Defects on Electrochemical Performance of Lithium-Ion Batteries: Cognizance of the Battery Failure Sources." *J. Power Sources*, **312** 70–79 (2016)
4. Ruschak, KJ, "Limiting Flow in a Pre-metered Coating Device." *Chem. Eng. Sci.*, **31** (11) 1057–1060 (1976)
5. Landau, L, Levich, B, "Dragging of a Liquid by a Moving Plate." *Acta Physicochim. URSS*, **17** 42–54 (1942)
6. Higgins, BG, Scriven, LE, "Capillary Pressure and Viscous Pressure Drop Set Bounds on Coating Bead Operability." *Chem. Eng. Sci.*, **35** (3) 673–682 (1980)
7. Koh, HJ, Kwon, I, Jung, HW, et al. "Operability Window of Slot Coating Using Viscocapillary Model for Carreau-Type

Coating Liquids.'' *Korea Aust. Rheol. J.*, **24** (2) 137–141 (2012)
8. Lee, SH, Koh, HJ, Ryu, BK, et al. ''Operability Coating Windows and Frequency Response in Slot Coating Flows from a Viscocapillary Model.'' *Chem. Eng. Sci.*, **66** (21) 4953–4959 (2011)
9. Tsuda, T, ''Coating Flows of Power-Law Non-Newtonian Fluids in Slot Coating.'' *Nihon Reoroji Gakkaishi*, **38** (45) 223–230 (2011)
10. Jang, I, Song, S, ''A Model for Prediction of Minimum Coating Thickness in High Speed Slot Coating.'' *Int. J. Heat Fluid Flow*, **40** 180–185 (2013)
11. Yoon, J, Kim, D, Lee, SH, et al. ''Simplified Model for Operability Window of Slot Coating Without Vacuum.'' *Chem. Eng. Sci.*, **259** 117766 (2022)
12. Carvalho, MS, Kheshgi, HS, ''Low-Flow Limit in Slot Coating: Theory and Experiments.'' *AICHE J.*, **46** (10) 1907–1917 (2000)
13. Chang, YR, Chang, HM, Lin, CF, et al. ''Three Minimum Wet Thickness Regions of Slot Die Coating.'' *J. Colloid Interface Sci.*, **308** (1) 222–230 (2007)
14. Kwak, H, Nam, J, ''Effect of Slot-Die Configurations on Coating Gap Dependence of Maximum and Minimum Wet Thicknesses.'' *AICHE J.*, **68** e17745 (2022)
15. Malakhov, R, Tjiptowidjojo, K, Schunk, PR, ''Mechanics of the Low-Flow Limit in Slot-Die Coating with No Vacuum.'' *AICHE J.*, **65** (6) e16593 (2019)
16. Lee, SH, Kim, SJ, Nam, J, et al. ''Effect of Sloped Die Lip Geometry on the Operability Window in Slot Coating Flows Using Viscocapillary and Two-dimensional Models.'' *J. Coat. Technol. Res.*, **11** (1) 47–55 (2014)
17. Ahn, WG, Lee, SH, Nam, J, et al. ''Effect of Upstream Meniscus Shape on Dynamic Wetting and Operating Limits of Newtonian Coating Liquids in Slot Coating Bead Flows.'' *J. Coat. Technol. Res.*, **15** (5) 1067–1076 (2018)
18. Tan, P, Diao, S, Huang, T, et al. ''Mechanism and Control of the Trailing Edge in Intermittent Slot Die Coating.'' *Ind. Eng. Chem. Res.*, **59** (35) 15758–15767 (2020)
19. Bhamidipati, KL, ''Detection and Elimination of Defects During Manufacture of High-temperature Polymer Electrolyte Membranes.'' Dissertation, Georgia Institute of Technology (2011)
20. Bhamidipati, KL, Harris, TAL, ''Numerical Simulation of a High Temperature Polymer Electrolyte Membrane Fabrication Process.'' *J. Fuel Cell Sci. Technol.*, **7** (6) 061005 (2010)
21. Huang, T, Tan, P, Zhong, Z, et al. ''Numerical and Experimental Investigation on the Defect Formation in Lithium-Ion-Battery Electrode-Slot Coating.'' *Chem. Eng. Sci.*, **258** 117744 (2022)
22. Kim, S, Lee, J, Lee, C, ''Computational Fluid Dynamics Model for Thickness and Uniformity Prediction of Coating Layer in Slot-Die Process.'' *Int. J. Adv. Manuf. Technol.*, **104** (5) 2991–2997 (2019)
23. Jung, H, Nam, J, ''Numerical Analysis of Pulsatile Flows in a Slot-Die Manifold.'' *J. Coat. Technol. Res.*, **16** (4) 1141–1151 (2019)
24. Schmitt, M, Baunach, M, Wengeler, L, et al. ''Slot-die Processing of Lithium-Ion Battery Electrodes-Coating Window Characterization.'' *Chem. Eng. Process.*, **68** 32–37 (2013)
25. Kwade, A, Haselrieder, W, Leithoff, R, et al. ''Current Status and Challenges for Automotive Battery Production Technologies.'' *Nat. Energy*, **3** (4) 290–300 (2018)
26. Pan, W, Chen, Z, Chen, X, et al. ''Slot Die Coating Window for a Uniform Fuel Cell Ink Dispersion.'' *AICHE J.*, **68** e17719 (2022)
27. Siqueira, IR, Carvalho, MS, ''A Computational Study of the Effect of Particle Migration on the Low-Flow Limit in Slot Coating of Particle Suspensions.'' *J. Coat. Technol. Res.*, **16** (6) 1619–1628 (2019)
28. de Araujo, SB, Carvalho, MS, ''Sedimentation and Marangoni Stress in Slot Coating Flow of Particle Suspension.'' *J. Non Newton. Fluid Mech.*, **247** 53–61 (2017)
29. Rebouças, RB, Siqueira, IR, Carvalho, MS, ''Slot Coating Flow of Particle Suspensions: Particle Migration in Shear Sensitive Liquids.'' *J. Nonnewton. Fluid Mech.*, **258** 22–31 (2018)
30. Hirt, CW, Nichols, BD, ''Volume of Fluid (VOF) Method for the Dynamics of Free Boundaries.'' *J. Comput. Phys.*, **39** (1) 201–225 (1981)
31. Schmitt, M, Scharfe, P, Schabel, W, ''Slot Die Coating of Lithium-Ion Battery Electrodes: Investigations on Edge Effect Issues for Stripe and Pattern Coatings.'' *J. Coat. Technol. Res.*, **11** (1) 57–63 (2014)
32. Blake, TD, Dobson, RA, Ruschak, KJ, ''Wetting at High Capillary Numbers.'' *J. Colloid Interface Sci.*, **279** (1) 198–205 (2004)
33. Spiegel, S, Heckmann, T, Altvater, A, et al. ''Investigation of Edge Formation During the Coating Process of Li-Ion Battery Electrodes.'' *J. Coat. Technol. Res.*, **19** (1) 121–130 (2022)
34. Higgins, BG, *The Physics of the Viscocapillary Coating Bead*. Convertech (2001)
35. Kwak, H, Nam, J, ''Simple Criterion for Vortex Formation in the Channel Flow of Power-Law Fluids.'' *J. Nonnewton. Fluid Mech.*, **284** 104372 (2020)